



CHEMISTRY & SUSTAINABILITY

# CHEM **SUS** CHEM

ENERGY & MATERIALS

## Accepted Article

**Title:** Ruthenium supported on High Surface Area Zirconia as an Efficient Catalyst for the Base-Free Oxidation of 5-Hydroxymethylfurfural to 2,5-Furandicarboxylic Acid

**Authors:** Christian M Pichler, Mohammad Ghith Al-Shaal, Dong Gu, Hrishikesh Joshi, Wirawan Ciptonugroho, and Ferdi Schüth

This manuscript has been accepted after peer review and appears as an Accepted Article online prior to editing, proofing, and formal publication of the final Version of Record (VoR). This work is currently citable by using the Digital Object Identifier (DOI) given below. The VoR will be published online in Early View as soon as possible and may be different to this Accepted Article as a result of editing. Readers should obtain the VoR from the journal website shown below when it is published to ensure accuracy of information. The authors are responsible for the content of this Accepted Article.

**To be cited as:** *ChemSusChem* 10.1002/cssc.201800448

**Link to VoR:** <http://dx.doi.org/10.1002/cssc.201800448>

WILEY-VCH

[www.chemsuschem.org](http://www.chemsuschem.org)

A Journal of



# Ruthenium supported on High Surface Area Zirconia as an Efficient Catalyst for the Base-Free Oxidation of 5-Hydroxymethylfurfural to 2,5-Furandicarboxylic Acid

Christian M. Pichler,<sup>†[a]</sup> Mohammad G. Al-Shaal,<sup>†[a]</sup> Dong Gu,<sup>[b]</sup> Hrishikesh Joshi,<sup>[a]</sup> Wirawan Ciptonugroho<sup>[c][d]</sup> and Ferdi Schüth<sup>\*[a]</sup>

<sup>†</sup> These authors contributed equally to this work

**Abstract:** Different ZrO<sub>2</sub> supported ruthenium catalysts were prepared and utilized in the oxidation of 5-hydroxymethylfurfural (HMF) to 2,5-furandicarboxylic acid (FDCA) under base-free conditions. Full conversion of HMF and almost perfect selectivity towards FDCA (97%) were achieved after 16 h, using pure O<sub>2</sub> as an oxidant and water as a solvent. The catalytic tests show that the size of the Ru particles is crucial for the catalytic performance and that the utilization of high surface area ZrO<sub>2</sub> leads to formation of very small Ru particles. Superior activity was obtained for catalysts based on ZrO<sub>2</sub> that had been synthesized by a surface casting method and possesses high surface areas up to 256 m<sup>2</sup> g<sup>-1</sup>. In addition to good activity and selectivity, these catalysts show also high stability and constant activity upon recycling, confirming the suitability of Ru/ZrO<sub>2</sub> in the base-free oxidation of HMF.

## Introduction

The intensive research on biomass valorization over the last decade shows the importance of biomass as sustainable feedstock not only in the energy sector but also in the production of chemicals.<sup>[1]</sup> Numerous bulk and fine chemicals, which are finding wide applications, can be derived from biomass and are used as alternatives for those produced from fossil resources.<sup>[2]</sup> One of the most promising chemicals for implementation in the chemical industry is 2,5-furandicarboxylic acid (FDCA), which is derived from the key platform molecule 5-hydroxymethylfurfural (HMF).<sup>[3–5]</sup> The high interest in FDCA results from the fact that it can be used for the synthesis of polymers. Due to its molecular similarity to terephthalic acid, FDCA can be used as a monomer in the production of bio-based polymers and composites.<sup>[6–9]</sup> The

polymer generated by reacting FDCA with ethane-1,2-diol, known as polyethylene furanoate (PEF), shows not only similar mechanical and physical properties as the conventional polyethylene terephthalate, but also superior barrier properties against H<sub>2</sub>O, CO<sub>2</sub>, and O<sub>2</sub>, which are crucial parameters for further application of PEF in grocery and beverage packaging.<sup>[10]</sup>

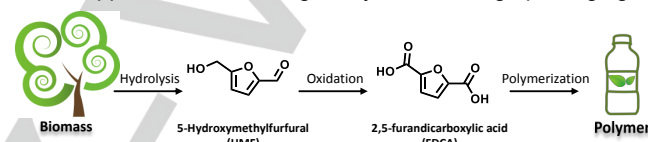


**Figure 1.** Schematic representation of polymer production starting from biomass via HMF and FDCA as intermediates.

A recent collaboration of the Coca Cola Company together with Avantium, Danone and ALPLA for commercialization of PEF based bottles underlines the high commercial potential of PEF and thereby FDCA.<sup>[11]</sup> Furthermore, PEF can be enzymatically degraded to yield the starting materials, which offers a novel recycling pathway.<sup>[12]</sup> The already existing commercial interest and the possibility to use biomass as feedstock make FDCA an attractive target molecule. Biomass-derived FDCA can be prepared through catalytic oxidation of HMF (Figure 1). Different oxidizing agents have been reported for this process, such as KMnO<sub>4</sub>,<sup>[13]</sup> peroxides,<sup>[14,15]</sup> and molecular oxygen (pure or in air).<sup>[16–19]</sup> Oxygen is the best studied oxidant, as it offers a clean, cheap, and efficient pathway for HMF oxidation. Numerous catalytic systems were developed and applied to enable the transformation of HMF to FDCA.<sup>[11]</sup> Electro- and photocatalysis,<sup>[16,20,21]</sup> homogeneous as well as heterogeneous catalysis<sup>[22,23]</sup> and also biocatalysis<sup>[15]</sup> were utilized for this task. Heterogeneous catalysis is the most commonly used method in HMF oxidation due to its cost effectiveness and the facile separation of product from catalyst. Noble metals such as Pt,<sup>[17,24–27]</sup> Pd,<sup>[28–31]</sup> Au,<sup>[32–35]</sup> Ru,<sup>[33,34]</sup> and alloys thereof performed best in terms of activity.<sup>[39,40]</sup> However, a major drawback of many of the aforementioned systems is the need of several equivalents of base in the reaction mixture. This requires subsequent neutralization of the reaction solution and separation of the formed salts, which both have a negative effect on the economy of the process and make it less eco-friendly. This fact triggered the development of base-free catalytic systems.<sup>[41–45]</sup> Ruthenium catalysts have been repeatedly reported as efficient catalysts for the base-free oxidation of HMF into DFF and FDCA.<sup>[46–48]</sup> The materials that have been used so far as supports for Ru can be mainly classified into carbon based materials and metal oxides.

[a] C. M. Pichler, Dr. M. G. Al-Shaal, H. Joshi, Prof. Dr. F. Schüth  
Max-Planck-Institut für Kohlenforschung  
Kaiser-Wilhelm-Platz 1, 45470 Mülheim an der Ruhr (Germany)  
E-mail: [schueth@kofo.mpg.de](mailto:schueth@kofo.mpg.de)

[b] Dr. D. Gu  
The Institute for Advanced Studies, Wuhan University, Wuhan,  
Hubei 430072, P.R. China

[c] Dr. W. Ciptonugroho  
Group of Inorganic Chemistry and Catalysis  
University Utrecht  
Universiteitsweg 99, 3584 CG Utrecht (Netherlands)

[d] Dr. W. Ciptonugroho  
Chemical Engineering Department of Sebelas Maret University,  
Jalan Ir. Sutami 36, A 51726 Surakarta, Indonesia

Supporting information for this article is given *via* a link at the end of the document.

Ruthenium supported on activated carbon exhibited activity for HMF oxidation and yielded 88% of FDCA (2 bar O<sub>2</sub>, 120 °C, and 10 h). However, the molar ratio of Ru to HMF was found to be lower than in comparable studies (ratio of 10 vs. 30-40 in comparable studies).<sup>[46]</sup> Polymer based materials featuring a triazine backbone structure were tested. In these materials the Ru nanoparticles are stabilized by interactions between the metal and the nitrogen containing moieties in the polymer.<sup>[47]</sup> The achieved yield of FDCA was 77% (at 20 bar O<sub>2</sub>, 140 °C and 1h). The issue observed in this study was the incomplete carbon balance, due to the strong interaction between the support and the reaction components. As an alternative various metal oxides can be applied as support, which also exhibited a strong influence on the resulting FDCA yields.<sup>[48]</sup> Depending on the utilized oxide FDCA yields varied between 20 and 100% (at 2.5 bar O<sub>2</sub>, 140 °C and 6h). The best results were obtained for Ru supported on several magnesium containing oxides, which acted as a solid base. However, Mg<sup>2+</sup> ions were found in the reaction solution, indicating that leaching occurs during the reaction and that the stability of the catalyst under the reaction conditions appears to be limited.

The previous examples clearly demonstrate that Ru is a highly active metal for the oxidation of HMF. However, there is a need to develop new supports that show high stability as well as low interaction with the reaction components, while simultaneously enabling high catalytic activity in combination with Ru. By taking these factors in consideration, ZrO<sub>2</sub> appears to be a highly attractive option. The high mechanical stability and low chemical reactivity make ZrO<sub>2</sub> a frequently used support in chemical industry. Increasing the surface area of this support would be another advantage that could potentially enhance the catalytic activity. Nevertheless, the preparation of high surface area ZrO<sub>2</sub> is still challenging, as mechanisms related to sintering can lead to a remarkable loss of surface area, especially during calcination and other necessary heat treatments. The first goal of this study was the synthesis of ZrO<sub>2</sub> supports with high surface areas by following our recently developed surface casting method.<sup>[49]</sup> To enable the comparison of the catalytic activity with established Ru/ZrO<sub>2</sub> catalysts, also other types of ZrO<sub>2</sub> have been used as supports for Ru catalysts. Tetragonal and monoclinic commercial ZrO<sub>2</sub>, in addition to a soft templated one, were used as supports for Ru catalysts and tested alongside Ru-supported on surface casted ZrO<sub>2</sub> in the aqueous oxidation of HMF to FDCA. Finally, the most active catalyst was further tested in order to determine its stability and recyclability.

## Results and Discussion

### Catalysts preparation

Different kinds of ZrO<sub>2</sub> were synthesized and used as supports for Ru based catalysts. Synthetic details are reported in the experimental section. Two different high surface area ZrO<sub>2</sub> supports were prepared *via* a surface casting method which

uses different kinds of silica as hard templates, namely, silanol-group-rich SBA-15 and aerogel. Different to conventional hard-templating pathways using silica templates, the silanol group-rich silica creates a strong interaction between the ZrO<sub>2</sub> precursor, ZrOCl<sub>2</sub>·8H<sub>2</sub>O, and the silica surface. This interaction then leads to the formation of a thin layer of oxide on the silica pore surface analogous to the synthesis of CMK-5 carbon. The preparation of the material is straightforward and employs a dry impregnation of the silica template with a solution of ZrOCl<sub>2</sub>·8H<sub>2</sub>O, followed by sequential heat treatments and template removal, as we reported previously.<sup>[49]</sup> The resulting material is denoted as ZrO<sub>2</sub> H-SBA.

Characterization of the resulting ZrO<sub>2</sub> material shows a hollow tubular array structure (Figure S1) with a surface area of 321 m<sup>2</sup> g<sup>-1</sup> (Figure S2).

In addition to ZrO<sub>2</sub> H-SBA, a second high surface area ZrO<sub>2</sub> support was prepared by using silanol-rich SiO<sub>2</sub> aerogel as template in the surface casting process.<sup>[50]</sup> In fact, the use of SiO<sub>2</sub> aerogels as template in the preparation of ZrO<sub>2</sub> is advantageous, as the synthesis of aerogel does not require surfactants, which have to be removed later, like in the case of SBA-15. The resulting calcined ZrO<sub>2</sub> (denoted as ZrO<sub>2</sub> H-aero) has a surface area of 375 m<sup>2</sup> g<sup>-1</sup>. This is considerably higher compared to other ZrO<sub>2</sub> materials obtained *via* the conventional hard templating methods (220 m<sup>2</sup> g<sup>-1</sup>).<sup>[51]</sup>

As an alternative to the surface casting approach, a soft templating technique was used to prepare a third type of ZrO<sub>2</sub>. For the so called EISA (evaporation-induced self-assembly) method, the surfactant F127 served as structure directing agent and Zr(OBu)<sub>4</sub> as a zirconia precursor. The synthesis route starts with a hydrolysis/condensation step, and after several drying and calcination steps, which are necessary to remove the surfactant, the final soft templated ZrO<sub>2</sub> support (denoted as ZrO<sub>2</sub> soft) was obtained, with a surface area of 41 m<sup>2</sup> g<sup>-1</sup>, which is significantly lower than the surface areas of the prepared hard templated ZrO<sub>2</sub>. Finally, two commercial ZrO<sub>2</sub> materials that differed in their crystal structure (monoclinic with S<sub>BET</sub> of 90 m<sup>2</sup> g<sup>-1</sup> and tetragonal with S<sub>BET</sub> of 133 m<sup>2</sup> g<sup>-1</sup>) were also chosen as supports for Ru catalysts.

The final Ru/ZrO<sub>2</sub> catalysts based on different ZrO<sub>2</sub> materials as supports, were prepared *via* a wet impregnation method. The aforementioned supports were dispersed in an ethanolic solution of RuCl<sub>3</sub>·xH<sub>2</sub>O prior to the removal of the solvent. Finally, the catalysts were reduced under H<sub>2</sub> atmosphere. The prepared catalysts were labelled Ru/ZrO<sub>2</sub> H-aero, Ru/ZrO<sub>2</sub> H-SBA, Ru/ZrO<sub>2</sub> soft, Ru/ZrO<sub>2</sub> C-mono and Ru/ZrO<sub>2</sub> C-tet.

### Characterization of catalysts

**Table 1.** Specific surface area, total pore volume and Ru content of the metal loaded Ru/ZrO<sub>2</sub> catalysts

Entry	Catalyst	S <sub>BET</sub> [m <sup>2</sup> ·g <sup>-1</sup> ] <sup>[a]</sup>	V <sub>P(total)</sub> <sup>[b]</sup>	Ru[wt.%] <sup>[c]</sup>
1	Ru/ZrO <sub>2</sub> H-aero	239	0.60	4.9
2	Ru/ZrO <sub>2</sub> H-SBA	256	0.25	5.2
3	Ru/ZrO <sub>2</sub> soft	37	0.05	4.8
4	Ru/ZrO <sub>2</sub> C-mono	86	0.25	5.4
5	Ru/ZrO <sub>2</sub> C-tet	103	0.14	5.0

[a] Surface area determined by the BET method. [b] Total pore volume determined at p/p<sub>0</sub> = 0.98. [c] Determined by ICP-OES.

Textural properties of the catalysts were characterized by N<sub>2</sub> physisorption. Comparison of the Brunauer-Emmett-Teller (BET)-surface areas of the prepared Ru-catalysts (Table 1), shows that the catalysts based on the surface casted ZrO<sub>2</sub> exhibit significantly higher S<sub>BET</sub> than the catalysts with soft templated and commercial supports (Table 1, entries 1,2 vs. 3-5). The Ru contents of the samples listed in Table 1 were determined by ICP-OES elemental analysis and were always in the range between 4 and 5% (Table 1, entries 1-5).

To gain further insight into the structure of the catalysts, they were analysed by TEM. Figure 2 shows the micrographs of the surface casted Ru/ZrO<sub>2</sub> catalysts (Ru/ZrO<sub>2</sub> H-aero (Figure 2, A) and Ru/ZrO<sub>2</sub> H-SBA (Figure 2, B)). Almost no Ru nanoparticles are observed on the surface of the support. This is most likely due to the fine distribution of very small particles and/or clusters over the surface of ZrO<sub>2</sub>. Furthermore, the unfavorable contrast between the metal and the support impedes the detection of small metal nanoparticles.<sup>[52,53]</sup> TEM analysis for Ru/ZrO<sub>2</sub> C-mono and Ru/ZrO<sub>2</sub> C-tet reveals the presence of Ru nanoparticles in the range of 2-3 nm (Figure S4 and S5). Finally, a TEM analysis of Ru/ZrO<sub>2</sub> soft gives similar results to those obtained from Ru/ZrO<sub>2</sub> H-aero and Ru/ZrO<sub>2</sub> H-SBA, where no Ru nanoparticles can be observed on the surface of the support (Figure S6).

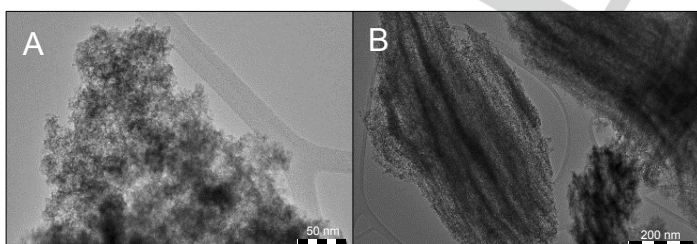


**Figure 2.** TEM images of: A) Ru/ZrO<sub>2</sub> H-aero; B) Ru/ZrO<sub>2</sub> H-SBA;

To overcome the difficulties caused by the low contrast in TEM analysis, Ru/ZrO<sub>2</sub> H-aero was further investigated using energy dispersive X-ray (SEM-EDX) analysis. Although SEM-EDX analysis can only provide a rough estimation of the size of Ru nanoparticles, element mapping, by which Ru is artificially

colored, can provide additional information on the distribution of the metal on the surface of the support. Ru/ZrO<sub>2</sub> H-aero shows a uniform allocation of Ru, excluding the formation of single big Ru particles (Figure 3) and confirming the distribution of Ru over the whole surface of ZrO<sub>2</sub>. A similar result is found for the other surface casted catalyst Ru/ZrO<sub>2</sub> H-SBA, where the Ru is also exhibiting a uniform distribution over the ZrO<sub>2</sub> support. (Figure S7).

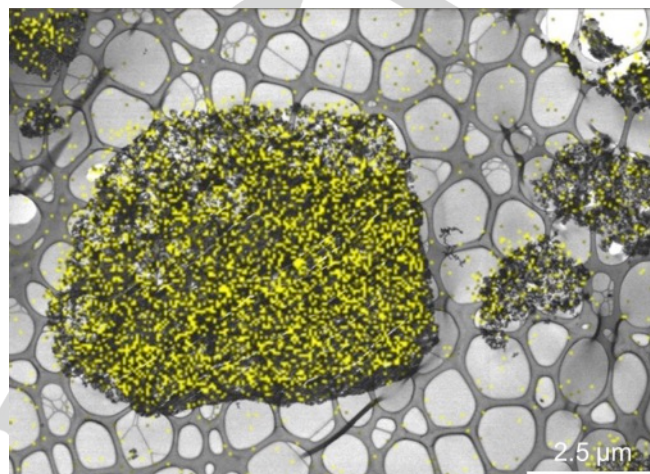


**Figure 3.** SEM-EDX element mapping of Ru/ZrO<sub>2</sub> H-aero (Ru is colored yellow).

XRD analysis confirms the conclusions that were drawn from the TEM and SEM-EDX micrographs. The XRD patterns for both Ru/ZrO<sub>2</sub> H-aero and Ru/ZrO<sub>2</sub> H-SBA show overall broad and low intensity reflections (Figure S10). The two broad reflections at 20-38° and 40-70° can be attributed to ZrO<sub>2</sub>. This indicates that ZrO<sub>2</sub> consists of very small crystalline domains.<sup>[49]</sup> In fact, the broadness of these features prevents any unambiguous crystal phase assignment. An additional small feature with low intensity can be recognized in the range of 40-45°. This can be attributed to the Ru<sup>0</sup> nanoparticles.<sup>[36]</sup> Nevertheless, the broadness of this reflection indicates the presence of very small Ru nanoparticles. In the case of the XRD patterns of Ru/ZrO<sub>2</sub> soft, Ru/ZrO<sub>2</sub> C-mono, and Ru/ZrO<sub>2</sub> C-tet, strong reflections related to different ZrO<sub>2</sub> crystalline phases were observed. Reflections at 24, 28, 31, 34, 40, 50, 54 and 63°, which belong to the monoclinic phase, were observed for Ru/ZrO<sub>2</sub> C-mono, whereas reflections at 30, 35, 50, 60 and 82°, which identify the tetragonal phase, were found for Ru/ZrO<sub>2</sub> soft and Ru/ZrO<sub>2</sub> C-tet. The sharpness and high intensity of the ZrO<sub>2</sub> reflections of all three materials indicate a high degree of crystallinity and rather large particles of ZrO<sub>2</sub>. However, the high intensity of ZrO<sub>2</sub> reflections makes the observation of any reflections related to Ru nanoparticles very difficult.

Due to the fact that it was not possible to directly observe Ru nanoparticles for Ru/ZrO<sub>2</sub> H-aero, Ru/ZrO<sub>2</sub> H-SBA, and Ru/ZrO<sub>2</sub> soft using TEM, and because furthermore the size estimation of Ru nanoparticles using SEM-EDX or XRD would be very inaccurate, hydrogen temperature programmed desorption (TPD) was performed in order to estimate the particle size of Ru in these

**Table 2.** HMF oxidation over different Ru/ZrO<sub>2</sub> catalysts.<sup>[a]</sup>

Entry	Catalyst	HMF conv. [%]	Selectivity [%]			Carbon balance [%] <sup>[b]</sup>
			DFF	FFCA	FDCA	
1	ZrO <sub>2</sub> H-aero	3	3	0	0	99
2	Ru/ZrO <sub>2</sub> H-aero	100	0	3	97	99
3	Ru/ZrO <sub>2</sub> H-SBA	97	0	13	87	99
4	Ru/ZrO <sub>2</sub> soft	95	26	45	19	98
5	Ru/ZrO <sub>2</sub> C-mono	99	4	36	60	99
6	Ru/ZrO <sub>2</sub> C-tet	100	6	40	54	99
7	1 % Ru/ZrO <sub>2</sub> H-aero	97	22	47	28	99
8	Ru/ZrO <sub>2</sub> H-aero 450	100	0	29	71	93

[a] Reaction conditions: HMF (63 mg, 0.5 mmol); Cat. (33 mg, 5% Ru loading equals 0.016 mmol Ru); 10 bar O<sub>2</sub>; 10 mL H<sub>2</sub>O; 120 °C; 500 rpm; and 16 h reaction time). [b] Carbon balance [%]=100-(HMF conversion-Σyields of DFF, FFCA, and FDCA).

materials. The calculated size of the Ru particles in Ru/ZrO<sub>2</sub> H-aero, Ru/ZrO<sub>2</sub> H-SBA was determined to be in the range of 0.8-1nm. In order to confirm the reliability of these findings, also Ru/ZrO<sub>2</sub> C-mono was analyzed by means of TPD as a reference material. The Ru particle size for this material was determined to be about 1.5 nm. This is close to the particle size determined by TEM analysis (Figure S4 and S5), which confirms the validity of the results obtained by TPD (Figure S8 and Table S9). The calculated particle size for Ru/ZrO<sub>2</sub> soft is significantly higher, at 3-4 nm.

### Catalytic oxidation of HMF to FDCA

The prepared catalysts were tested in the base-free oxidation of HMF to FDCA. Conditions were chosen to correspond to those reported in literature.<sup>[11,47]</sup> Neat O<sub>2</sub> was used as an oxidant (10 bar) and 120 °C was applied to enable the conversion of HMF to FDCA. Water was used as a solvent and the HMF/metal-ratio in all tests was 36.5:1. Under these conditions and in the absence of any base, HMF is oxidized firstly to 2,5-diformylfuran (DFF), which undergoes a subsequent oxidation reaction to yield 5-formyl-2-furan carboxylic acid (FFCA) and ultimately FDCA (Figure 4).<sup>[11,43]</sup> In the first test, HMF oxidation was investigated over a blank ZrO<sub>2</sub> H-aero support. After 16 h, only 3% conversion of HMF to DFF was obtained, highlighting the need for Ru in the oxidation reactions (Table 2, entry 1). Oxidation of HMF with both Ru on surface casted ZrO<sub>2</sub> catalysts, namely, Ru/ZrO<sub>2</sub> H-aero and Ru/ZrO<sub>2</sub> H-SBA, shows high activity and yields FDCA with high selectivity (Table 2, entries 2,3 and Figure 5). Although full conversion of HMF was observed over both catalysts, Ru/ZrO<sub>2</sub> H-aero seems to be more active than Ru/ZrO<sub>2</sub> H-SBA. This can be inferred from the significant drop in the concentration of DFF after 2 h and FFCA after 4 h over Ru/ZrO<sub>2</sub> H-aero (Figure 5a). In contrast, the yield of DFF decreases slowly after 4 h, while the yield of FFCA remains more or less constant over the time

between 4 and 12 h over Ru/ZrO<sub>2</sub> H-SBA (Figure 5b). After 12 h, a drop in the yield of FFCA occurs and FDCA becomes the main product in the reaction mixture. 84% yield of FDCA is achieved over Ru/ZrO<sub>2</sub> H-SBA while Ru/ZrO<sub>2</sub> H-aero enables a full conversion of HMF with 97% selectivity towards FDCA.

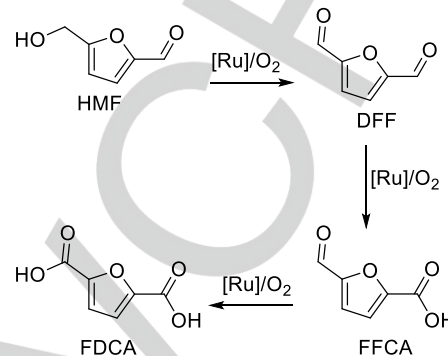


**Figure 4.** Reaction pathway of the base-free HMF oxidation to FDCA through DFF and FFCA as intermediates.

As both catalysts possess similar textural properties (Table 1, entries 1,2), the difference in the catalytic activity may be attributed to the morphology of the supports in both catalysts.

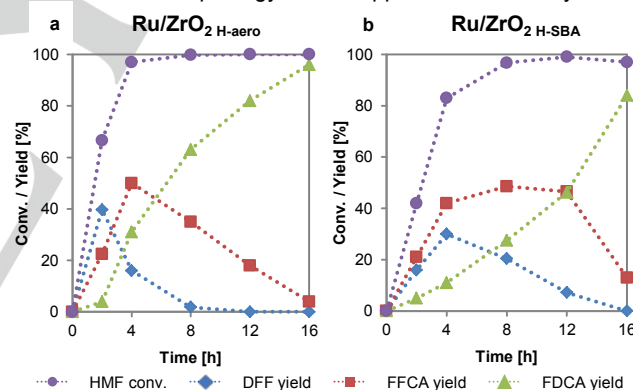


**Figure 5.** Oxidation of HMF over Ru/ZrO<sub>2</sub> H-aero (left) and Ru/ZrO<sub>2</sub> H-SBA (right). Reaction conditions: HMF (63 mg, 0.5 mmol); Cat. (33 mg, 0.016 mmol Ru); 10 bar O<sub>2</sub>; 10 mL H<sub>2</sub>O; 120 °C; 500 rpm; Yields are given in mol%.

For the Ru-impregnated on soft-templated support, Ru/ZrO<sub>2</sub> soft, lower activity in comparison to Ru/ZrO<sub>2</sub> H-aero and Ru/ZrO<sub>2</sub> H-SBA catalysts was observed (Table 2, entries 2,3 vs. 4). Although almost full conversion of HMF (95%) can be obtained after 16 h, the yield of FDCA does not exceed 19%, whereas the main product was FFCA with a yield of 45% (Figure S11). These findings prove the poor activity of Ru/ZrO<sub>2</sub> soft in the oxidation of HMF. It is reasonable to argue that the lower catalytic activity of Ru/ZrO<sub>2</sub> soft in comparison to Ru/ZrO<sub>2</sub> H-aero and Ru/ZrO<sub>2</sub> H-SBA is due to the significantly lower surface area of Ru/ZrO<sub>2</sub> soft (37 m<sup>2</sup> g<sup>-1</sup>), leading to a bigger size of the Ru nanoparticles (0.8 nm and 1.0 nm vs. 3.4 nm) (Table S9).

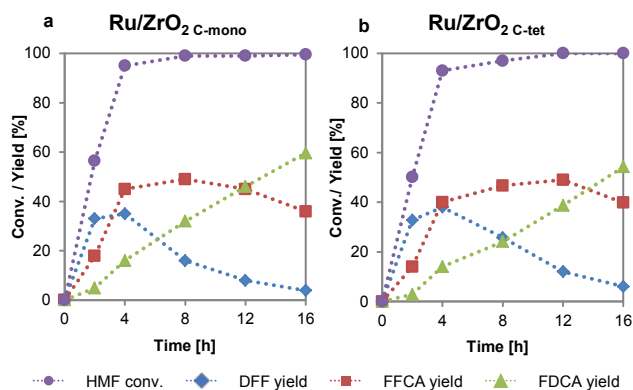


**Figure 6.** Oxidation of HMF over Ru/ZrO<sub>2</sub> C-mono (left) and Ru/ZrO<sub>2</sub> C-tet (right). Reaction conditions: HMF (63 mg, 0.5 mmol); Cat. (33 mg, 5% Ru loading equals 0.016 mmol Ru); 10 bar O<sub>2</sub>; 10 mL H<sub>2</sub>O; 120 °C; 500 rpm, Yields are given in mol%.

In order to investigate the influence of the crystalline phase of the ZrO<sub>2</sub> support on the catalyst performance, HMF oxidation was investigated over Ru supported on commercially available monoclinic and tetragonal ZrO<sub>2</sub> (Figure 6a and b). Interestingly, both catalysts, Ru/ZrO<sub>2</sub> C-mono and Ru/ZrO<sub>2</sub> C-tet, enable comparable activities and selectivity towards the intermediates and FDCA. 59% and 54% yields of FDCA were achieved after 16 h over Ru/ZrO<sub>2</sub> C-mono and Ru/ZrO<sub>2</sub> C-tet, respectively. The selectivity towards DFF and FDCA were also comparable in both cases. Evidently, these findings exclude any direct influence of the crystalline structure of the support on the catalytic activity in HMF oxidation. However, it can be seen that Ru/ZrO<sub>2</sub> C-mono and Ru/ZrO<sub>2</sub> C-tet have a considerably lower activity in comparison to the high surface materials, Ru/ZrO<sub>2</sub> H-aero and Ru/ZrO<sub>2</sub> H-SBA (Figure 5 vs. Figure 6). This can be related to the influence of the Ru nanoparticle size on the catalytic activity. Both catalysts, Ru/ZrO<sub>2</sub> H-aero and Ru/ZrO<sub>2</sub> H-SBA, possess high  $S_{\text{BET}}$  (> 200 m<sup>2</sup> g<sup>-1</sup>) which allows the distribution of Ru over a larger area and leads to the formation of small Ru nanoparticles (0.8 nm for Ru/ZrO<sub>2</sub> H-aero and 1.0 nm for Ru/ZrO<sub>2</sub> H-SBA, Table S9). This fact enables a quantitative conversion of HMF to FDCA. In contrast, Ru/ZrO<sub>2</sub> C-mono and Ru/ZrO<sub>2</sub> C-tet show relatively lower catalytic activity, corresponding to the larger size of Ru particles of 1.8 nm (Ru/ZrO<sub>2</sub> C-mono) and 1.5 nm (Ru/ZrO<sub>2</sub> C-tet). A further comparison of the catalytic activity between Ru/ZrO<sub>2</sub> soft and Ru/ZrO<sub>2</sub> C-tet confirms the effect of the Ru particle size on the catalytic activity. Although both catalysts share the tetragonal crystalline structure of ZrO<sub>2</sub>, the commercial catalyst shows better catalytic performance than Ru/ZrO<sub>2</sub> soft. While the yield of FDCA reaches 54% after 16 h over Ru/ZrO<sub>2</sub> C-tet with a Ru particle size of 1.5 nm, only 19% is achieved over Ru/ZrO<sub>2</sub> soft with a Ru particle size of 3.4 nm. Rate constants were also calculated for the particular catalysts and normalized to the Ru metal surface area (see Supporting Information, Table S16). The normalized rates (for all three reaction steps) are in a similar

range, emphasizing the significance of small Ru particles. The formation of small Ru nanoparticles is facilitated by high BET surface areas of the ZrO<sub>2</sub> support. The surface casted catalysts Ru/ZrO<sub>2</sub> H-aero and Ru/ZrO<sub>2</sub> H-SBA, show the highest BET surface areas, resulting in the highest catalytic activity among the tested materials in our study. The influence of Ru particle size is also found for materials with the same ZrO<sub>2</sub> support, but differently sized Ru particles. If the Ru impregnated support is reduced at higher temperatures, bigger Ru particles are formed (reduction at 450 °C leads to formation of Ru particles with an average size of 1.7 nm on ZrO<sub>2</sub> H-aero). The catalytic tests of this material yielded significantly less FDCA compared with the material reduced at 250 °C (Table 2, Entry 8 and Supporting Information Figure S18).

It was also tried to reduce the Ru loading of the most promising catalyst material, which is Ru/ZrO<sub>2</sub> H-aero. A catalyst with 1 wt.% Ru on ZrO<sub>2</sub> H-aero was prepared and tested for the HMF oxidation. The results (Table 2, Entry 7) show that full HMF conversion can be achieved, the yield of FDCA is, however, significantly lower. To obtain full yield of FDCA in an acceptable reaction time, 5 wt.% Ru loading seem to be appropriate.

As next step, recyclability tests were carried out to provide more insight into the reusability and the stability of these materials. The recyclability of Ru/ZrO<sub>2</sub> H-aero has been investigated over five consecutive runs where the reaction conditions were the same (HMF (63 mg, 0.5 mmol); catalyst (33 mg, 0.016 mmol Ru); 10 bar O<sub>2</sub>; 10 mL H<sub>2</sub>O; 120 °C; 500 rpm; and 1 h reaction time). Conducting the oxidation reaction over 1 h period affords incomplete conversion of HMF enabling better comparability between the different tests. As depicted in Figure 7, only a slight drop in the catalytic activity can be observed over the recycling runs. Most importantly, no loss in the carbon balance was observed upon recycling. 5% increase in the yield of DFF in the fifth cycle indicates a slight deactivation of Ru/ZrO<sub>2</sub> H-aero. An ICP-OES analysis of the reaction solutions after each test together with the catalyst after the fifth cycle reveal only a very limited loss of the Ru content (1 ppm).

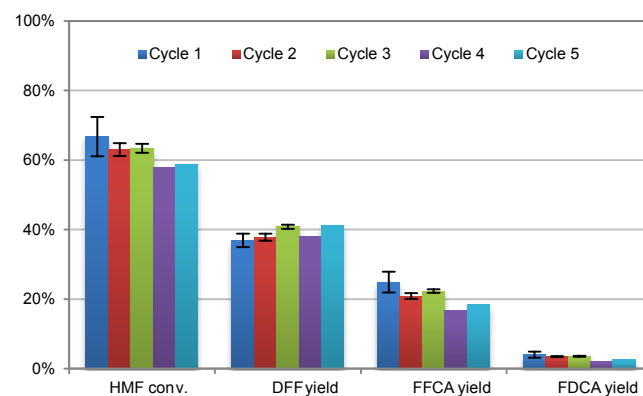


**Figure 7.** Recycling test over Ru/ZrO<sub>2</sub> H-aero. Reaction conditions: HMF (63 mg, 0.5 mmol); Cat. (33 mg, 0.016 mmol Ru); 10 bar O<sub>2</sub>; 10 mL H<sub>2</sub>O; 120 °C; 500 rpm; and 1 h reaction time, Yields are given in mol%.

The used catalysts after the 5<sup>th</sup> recycle were further characterized by XRD analysis (Figure S12). A clear change in the reflections attributed to the support can be seen for the recycled material. This is most obvious for the reflections at 30 and 50° and is explained by the increased crystallinity of ZrO<sub>2</sub>. The features attributed to Ru, in the range of 40–45°, are very broad with low intensity. This indicates no growth in Ru particles upon recycling. TEM analysis of the recycled catalysts confirms the conclusions drawn from the XRD measurements. The crystallinity of the ZrO<sub>2</sub> has increased during the recycling tests, whereas the Ru clusters are still not visible on the high surface ZrO<sub>2</sub> support. (Figure S14).

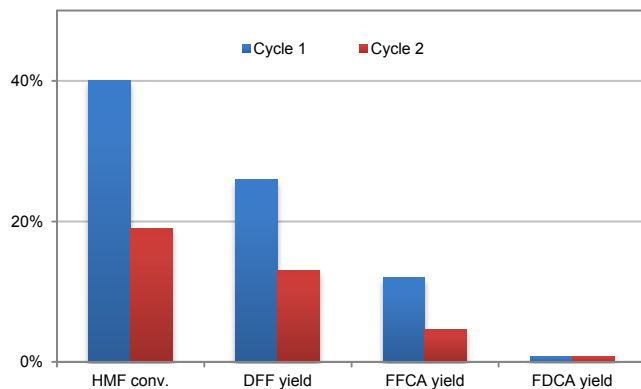


**Figure 8.** Recycling test over Ru/ZrO<sub>2</sub> H-SBA. Reaction conditions: HMF (63 mg, 0.5 mmol); Cat. (33 mg, 0.016 mmol Ru); 10 bar O<sub>2</sub>; 10 mL H<sub>2</sub>O; 120 °C; 500 rpm; and 1 h reaction time. Yields are given in mol%.

In contrast to the catalyst based on the aerogel casted ZrO<sub>2</sub>, a recyclability test of Ru/ZrO<sub>2</sub> H-SBA reveals low structural stability, which is probably the reason for the lower catalytic activity upon recycling. Figure 8 shows that the conversion of HMF dropped from 40% over the fresh Ru/ZrO<sub>2</sub> H-SBA to 19% over the recycled one even after the first recycling run. This decrease in the conversion was accompanied with a drop in the yield of the intermediates and FDCA but with no loss in the carbon balance. TEM investigation of Ru/ZrO<sub>2</sub> H-SBA, before and after the reaction shows clearly a collapse of the tubular structure of the support, although no drastic change in the S<sub>BET</sub> was found for the fresh and the used catalyst (Figure S14 and Table S15). These findings confirm that the morphology of the supporting material has also a major impact on the catalytic activity. The changes in the structure of the support during the reaction can lead to a change in the catalytic activity. It can be considered, that a part of the Ru particles becomes inaccessible for the reactants through this major change in morphology. A growth of the Ru particles was not observed, for the used Ru/ZrO<sub>2</sub> H-SBA catalyst, as the H<sub>2</sub>-TPD measurement of the used catalyst gave similar results as for the fresh material (Table S9). Thus, the superiority of the relatively stable Ru/ZrO<sub>2</sub> H-aero in comparison to Ru/ZrO<sub>2</sub> H-SBA can be related to the collapse of the structure of Ru/ZrO<sub>2</sub> H-SBA that takes place during the oxidation reaction.

## Conclusions

In this study, we have introduced Ru supported on ZrO<sub>2</sub> as a catalyst with high potential in the oxidation of 5-hydroxymethylfurfural to 2,5-furandicarboxylic acid under base-free conditions. Different Ru/ZrO<sub>2</sub> catalysts, based on commercial ZrO<sub>2</sub> as well as ZrO<sub>2</sub> supports that were obtained via surface casting and soft templating, were prepared and tested in the oxidation of HMF. The small particle size of Ru and its fine dispersion over the support proved to be a key factor for high activity in the oxidation reaction. Small Ru nanoparticles can be obtained by using a high surface area ZrO<sub>2</sub> support material. Therefore, the surface casted ZrO<sub>2</sub> materials are especially well suited supports, as they exhibit a very high surface area. The Ru loaded catalysts based on these materials show, as expected, very small metal nanoparticles (0.8–1 nm), which proved to be highly beneficial for the catalytic performance. This demonstrates the benefits of using these novel surface casted materials as catalyst supports. Ru/ZrO<sub>2</sub> H-aero was identified as the most active catalyst in the oxidation of HMF and showed clearly better catalytic performance than catalysts based on commercial or soft templated ZrO<sub>2</sub>. The utilization of Ru/ZrO<sub>2</sub> H-aero enables full conversion of 5-hydroxymethylfurfural with a selectivity of 97% towards 2,5-furandicarboxylic acid at 120 °C under 10 bar of O<sub>2</sub>. Ru/ZrO<sub>2</sub> H-aero exhibits also high stability upon recycling. Furthermore, this catalyst does not show signs of leaching and also the carbon balances are closed, which eliminates significant issues that were observed with other Ru based catalyst systems.<sup>[47,48]</sup> Overall, the high activity together with high stability make Ru/ZrO<sub>2</sub> H-aero an excellent candidate for a sustainable production of 2,5-furandicarboxylic acid.

## Experimental Section

### Materials

All chemicals were purchased from commercial suppliers and used as received: tetraethylorthosilicate (Sigma-Aldrich, reagent grade 98%) Pluronic P123 (Sigma-Aldrich, average M<sub>n</sub> ≈ 5800) ZrOCl<sub>2</sub>·8H<sub>2</sub>O (Sigma-Aldrich, reagent grade 98%), 5-hydroxymethylfurfural (Sigma-Aldrich, 99%), RuCl<sub>3</sub>·xH<sub>2</sub>O (Sigma-Aldrich, ReagentPlus<sup>®</sup>), monoclinic ZrO<sub>2</sub> (Alfa Aesar, catalyst support). The tetragonal ZrO<sub>2</sub> was supplied by Saint-Gobain NorPro (type SZ6\*152 with an impurity of 3.3 % SiO<sub>2</sub>). ZrO<sub>2</sub> was crushed and milled with a mortar and subsequently sieved. Only particles sized < 50 μm were used.

### Preparation of Si-OH rich SBA-15

The preparation of silanol rich SBA-15 was performed according to literature.<sup>[49]</sup> Briefly, 20.0 g Pluronic P123 were dissolved in 650 mL H<sub>2</sub>O together with 37 wt.% HCl and heated under stirring at 38 °C. Following addition of 41.6 g tetraethylorthosilicate (TEOS) the solution was kept at 38 °C and stirred for 24 h. The resulting white suspension was hydrothermally treated at 110 °C for another 24 h. Filtration of the suspension yielded a white precipitate, which was dried at 80 °C for at least 12 h. To remove the P123 template 8.0 g of the solid was dispersed in 120 mL 65 wt.% HNO<sub>3</sub> and 40 wt.% H<sub>2</sub>O<sub>2</sub> (careful, highly corrosive) in

a 1 L round bottom flask and heated under stirring with a magnetic stirring bar at 80 °C. (The highly corrosive mixture releases brown NO<sub>x</sub> gases after a temperature of 80 °C was reached. The gases were absorbed in a 4 M NaOH solution). After 3 h the product was collected by filtration and thoroughly washed with water and ethanol and finally dried overnight at 50 °C.

#### Preparation of SiO<sub>2</sub> aerogel

The SiO<sub>2</sub> aerogel was prepared according to literature.<sup>[50]</sup> In a glass beaker 20.8 g TEOS was dissolved under stirring with a magnetic stirring bar in 99 mL ethanol. Then 7.2 g H<sub>2</sub>O was added and the pH value of the solution was adjusted to pH 3 by addition of 15 wt.% HCl, while monitoring the pH value with a pH electrode. The solution was stirred for 5 h 30 min. Afterwards the pH of the solution was adjusted to pH 7 by addition of 1 mol·L<sup>-1</sup> NH<sub>3</sub> solution and the stirring was stopped. The solution was aged by letting it stand for 14–16 h. After this time a gel had formed. This gel was subjected to drying with supercritical CO<sub>2</sub> with a CO<sub>2</sub> flow setup at 200 bar and 50 °C. The resulting product was a fine white powder.

#### Preparation of high surface area ZrO<sub>2</sub>

The preparation of high surface area ZrO<sub>2</sub> was performed according to literature.<sup>[49]</sup> At first 2.0 g ZrOCl<sub>2</sub>·8H<sub>2</sub>O was dissolved by heating to 50 °C in 1.5 g of 1.07 mol·L<sup>-1</sup> HCl. 0.5 g of silica template (SBA-15 or aerogel) was impregnated with the calculated amount of the above solution (15.6 wt.% calculated for ZrO<sub>2</sub> for SBA-15 and 14.5 wt.% calculated for ZrO<sub>2</sub> for SiO<sub>2</sub> aerogel). The impregnated material was sealed in a glass vial and aged at 50 °C for 24 h and 90 °C for 48 h, followed by calcination at 450 °C for 5 h (heating ramp 1 °C·min<sup>-1</sup>). To remove the SiO<sub>2</sub> template the calcined material was treated with 35 mL of 2 mol·L<sup>-1</sup> NaOH solution at 70 °C two times and finally washed with H<sub>2</sub>O and ethanol.

#### Preparation of soft templated ZrO<sub>2</sub>

The preparation of soft templated ZrO<sub>2</sub> was performed according to the literature-known EISA method.<sup>[54]</sup> In a glass beaker 2.44 g F127 and 1.54 g citric acid were dissolved in 74 mL ethanol while stirring with a magnetic stirring bar. Then 3.67 g HCl (37%) was added and 5.85 g zirconium(IV)butoxide was added dropwise into the homogeneous solution and stirred for 3 h until the solution became turbid. The obtained dispersion was poured into a petri dish to allow evaporation of the solvent for 48 h at room temperature. Afterwards the sample was dried at 100 °C and the obtained solid was calcined at 550 °C for 5 h (heating ramp 1 °C·min<sup>-1</sup>).

#### Preparation of impregnated ruthenium loaded catalyst

In a round bottom flask the calculated amount of RuCl<sub>3</sub>·xH<sub>2</sub>O was dissolved in ethanol (25 mL per 0.25 g ZrO<sub>2</sub>) and the desired ZrO<sub>2</sub> support was added and the suspension was stirred for 16 h. Then the solvent was removed by evaporation on the rotary evaporator and the material was dried at 95 °C for 48 h. Finally, the dry material was reduced in a tube furnace with pure H<sub>2</sub> at 250 °C for 3 h (heating ramp 1 °C·min<sup>-1</sup> and H<sub>2</sub> flow 33 mL·min<sup>-1</sup>). For the synthesis of samples with bigger Ru particles, the impregnated materials were reduced at 450 °C for 3 h.

#### Characterization

The powder X-ray diffraction (XRD) patterns were recorded on a Stoe  $\Theta$ - $\Theta$  diffractometer operating in reflection mode with Cu K $\alpha_{1,2}$  radiation that

was monochromatized with a secondary graphite monochromator. The nitrogen adsorption-desorption measurements were performed on a NOVA 3200e instrument at -195.8 °C. The transmission electron microscopy (TEM) images were taken with a Hitachi H-7100 and HF-2000 at an acceleration voltage of 100 or 200 kV. STEM images were recorded on a Hitachi HD-2700 dedicated Scanning Transmission Electron Microscope operated at 200 kV equipped with an EDAX Octane T Ultra W EDX detector. The ICP-OES measurements were conducted at micro analytic laboratory Kolbe (Mülheim an der Ruhr, Germany).

Temperature programmed desorption of hydrogen (TPD) was conducted on a Micromeritics AutoChem II (Chemisorption Analyzer). In the beginning 50 mL/min pure Ar stream was used to preheat approx. 50 mg catalyst at 300 °C for 15 min. After cooling down to 50 °C, 10% H<sub>2</sub> in Ar was passed through the sample and held for 10 min before heating to 250 °C with a heating rate of 1 °C/min. This temperature was held for 180 min to reduce the sample. Afterwards the gas flow was switched back to pure Ar while heating to 300 °C (3 °C/min). To remove all hydrogen this temperature was held for 60 min. Then the sample was cooled down to 50 °C and the gas was switched back to 10% H<sub>2</sub> in Ar and held at this temperature for 80 min so hydrogen could chemisorb on all metal particles. To remove the physisorbed hydrogen the sample was flushed with pure Ar for 60 min. The measurement itself was then performed by gradually heating the sample with a ramping rate of 10 °C/min up to 500 °C that all chemisorbed hydrogen will be removed from the metal surface. To quantify the amount of hydrogen desorbed during the heating of the samples, defined volumes of H<sub>2</sub> were injected in the TCD detector and plotted against the areas of the obtained peaks. The Ru particle size was determined by using the relation  $l=5/S*d$ , where  $l$  is the particle size,  $S$  is the metal surface area (that can be derived from the amount of desorbed hydrogen) and  $d$  is the density of ruthenium (12.3 g/cm<sup>3</sup>).<sup>[55,56]</sup>

#### Catalytic tests

The catalytic tests were performed in stainless-steel autoclaves (50 mL) with Teflon inlet and temperature and pressure sensing elements. The autoclave was charged with 10 mL of an aqueous HMF solution (0.05 mol·L<sup>-1</sup>) and 33 mg catalyst (molar ratio Ru:HMF = 31:1 for 5% Ru containing catalysts) and a magnetic stirring bar. Then the autoclave was sealed, flushed three times with O<sub>2</sub> and then pressurized to 10 bar with O<sub>2</sub>, heated to 120 °C with a metallic heating jacket and stirred at 500 rpm. After the designated time the autoclave was cooled in an ice bath, the pressure was released and the catalyst was removed by filtration. The filtrated catalyst was washed with methanol to remove also solid reaction products. Samples were taken from the aqueous reaction solution as well as from the methanolic washing solution and analyzed by HPLC on a Shimadzu LC20-Prominence chromatograph equipped with a 100 mm organic acid resin column with 8.0 mm i.d. and a precolumn (40 mm organic acid resin with 8.0 mm i.d.). As mobile phase an aqueous solution of trifluoroacetic acid (2 mmol·L<sup>-1</sup>) was used with a flow rate of 1 mL·min<sup>-1</sup> at a temperature of 40 °C. For detection an UV detector was used and external one point calibration was applied to quantify HMF, DFF, FFCA and FDCA.

The recyclability of the catalysts was tested in five consecutive runs. These tests were carried out under the same reaction conditions as stated above only with the reaction time fixed at 1 h. In the first recyclability run the reaction was carried out five times in parallel and the calculated conversions and yields were averaged. After the reaction the catalyst was filtered, washed with methanol and dried under vacuum at 50 °C and the materials from the single reactions were merged together before forwarding the material for the next run. In the subsequent runs the number of parallel reactions had to be reduced successively to compensate the loss of catalyst during recovery of the material. At the

fifth recyclability run only one reaction could be performed. Nevertheless this system assures that the conditions are the same for all of the reactions and no effects of down scaling or similar issues can influence the results.

## Acknowledgements

C. M. Pichler gratefully acknowledges financial support from the Marietta Blau-scholarship of the OeAD funded by the Austrian ministry of science, research and economics. We acknowledge Saint Gobain NorPro for the kind supply of ZrO<sub>2</sub> SZ6\*152. We thank Bernd Spliethoff and Hans-Josef Bongard for the TEM and STEM-EDX measurements, Laila Sarahoui for the skillful assistance in the performance of reaction tests and Prof. Rolf Breinbauer for helpful remarks and comments on the manuscript. This work was performed as part of the Cluster of Excellence "Tailor-Made Fuels from Biomass", which is funded by the Excellence Initiative by the German federal and state governments to promote science and research at German universities.

**Keywords:** 2,5-furandicarboxylic acid • high surface area ZrO<sub>2</sub> • surface casting • oxidation catalyst • ruthenium

## References

- [1] A. Corma Canos, S. Iborra, A. Velly, *Chem. Rev.* **2007**, *107*, 2411–2502.
- [2] P. Gallezot, *Chem. Soc. Rev.* **2012**, *41*, 1538–58.
- [3] R. S. M. Poliakoff, C.O. Tuck, E. Perez, I. Horvath, *Science* **2012**, *337*, 695–699.
- [4] J. S. Luterbacher, D. Martin Alonso, J. A. Dumesic, *Green Chem.* **2014**, *16*, 4816–4838.
- [5] M. J. Climent, A. Corma, S. Iborra, *Green Chem.* **2014**, *16*, 516–547.
- [6] A. Gandini, A. J. D. Silvestre, C. P. Neto, A. F. Sousa, M. Gomes, *J. Polym. Sci. Part A Polym. Chem.* **2009**, *47*, 295–298.
- [7] R. J. I. Knoop, W. Vogelzang, J. Van Haveren, D. S. Van Es, *J. Polym. Sci. Part A Polym. Chem.* **2013**, *51*, 4191–4199.
- [8] A. J. J. E. Eerhart, A. P. C. Faaij, M. K. Patel, *Energy Environ. Sci.* **2012**, *5*, 6407–6422.
- [9] S. Rajendran, R. Raghunathan, I. Hevus, R. Krishnan, A. Ugrinov, M. P. Sibi, D. C. Webster, J. Sivaguru, *Angew. Chemie - Int. Ed.* **2015**, *54*, 1159–1163.
- [10] E. De Jong, M. A. Dam, L. Sipos, G. J. M. Gruter, *ACS Symp. Ser.* **2012**, *1105*, 1–13.
- [11] Z. Zhang, K. Deng, *ACS Catal.* **2015**, *5*, 6529–6544.
- [12] A. Pellis, K. Haernvall, C. M. Pichler, G. Ghazaryan, R. Breinbauer, G. M. Guebitz, *J. Biotechnol.* **2015**, *235*, 47–53.
- [13] H. M. T. Miura, H. Kakinuma, T. Kawano, *US Pat. 7,411,078, B2* **2008**.
- [14] T. S. Hansen, I. Sádaba, E. J. García-Suárez, A. Riisager, *Appl. Catal. A Gen.* **2013**, *456*, 44–50.
- [15] W. P. Dijkman, D. E. Groothuis, M. W. Fraaije, *Angew. Chemie - Int. Ed.* **2014**, *53*, 6515–6518.
- [16] K. R. Vuyyuru, P. Strasser, *Catal. Today* **2012**, *195*, 144–154.
- [17] Y. Zhang, Z. Xue, J. Wang, X. Zhao, Y. Deng, W. Zhao, T. Mu, *RSC Adv.* **2016**, *6*, 51229–51237.
- [18] L. Ardemani, G. Cibin, A. J. Dent, M. A. Isaacs, G. Kyriakou, A. F. Lee, C. M. A. Parlett, S. A. Parry, K. Wilson, *Chem. Sci.* **2015**, *6*, 4940–4945.
- [19] C. V. Nguyen, Y.-T. Liao, T.-C. Kang, J. E. Chen, T. Yoshikawa, Y. Nakasaka, T. Masuda, K. C.-W. Wu, *Green Chem.* **2016**, *18*, 5957–5961.
- [20] H. G. Cha, K.-S. Choi, *Nat Chem* **2015**, *7*, 328–333.
- [21] B. You, N. Jiang, X. Liu, Y. Sun, *Angew. Chemie - Int. Ed.* **2016**, *55*, 9913–9917.
- [22] B. Saha, S. Dutta, M. M. Abu-Omar, *Catal. Sci. Technol.* **2012**, *2*, 79–81.
- [23] W. Partenheimer, V. V. Grushin, *Adv. Synth. Catal.* **2001**, *343*, 102–111.
- [24] Z. Miao, T. Wu, J. Li, T. Yi, Y. Zhang, X. Yang, *RSC Adv.* **2015**, *5*, 19823–19829.
- [25] H. Ait Rass, N. Essayem, M. Besson, *Green Chem.* **2013**, *15*, 2240.
- [26] H. Ait Rass, N. Essayem, M. Besson, *ChemSusChem* **2015**, *8*, 1206–1217.
- [27] P. Verdeguer, N. Merat, A. Gaset, *J. Mol. Catal.* **1993**, *85*, 327–344.
- [28] B. Liu, Y. Ren, Z. Zhang, *Green Chem.* **2015**, *17*, 1610–1617.
- [29] N. Mei, B. Liu, J. Zheng, K. Lv, D. Tang, Z. Zhang, *Catal. Sci. Technol.* **2015**, *5*, 3194–3202.
- [30] B. Siyo, M. Schneider, J. Radnik, M. M. Pohl, P. Langer, N. Steinfeldt, *Appl. Catal. A Gen.* **2014**, *478*, 107–116.
- [31] Z. Zhang, J. Zhen, B. Liu, K. Lv, K. Deng, *Green Chem.* **2015**, *17*, 1308–1317.
- [32] J. Cai, H. Ma, J. Zhang, Q. Song, Z. Du, Y. Huang, J. Xu, *Chemistry* **2013**, *19*, 14215–14223.
- [33] O. Casanova, S. Iborra, A. Corma, *ChemSusChem* **2009**, *2*, 1138–1144.
- [34] S. E. Davis, B. N. Zope, R. J. Davis, *Green Chem.* **2012**, *14*, 143–147.
- [35] S. E. Davis, L. R. Houk, E. C. Tamargo, A. K. Datye, R. J. Davis, *Catal. Today* **2011**, *160*, 55–60.
- [36] F. Kerdi, H. Ait Rass, C. Pinel, M. Besson, G. Peru, B. Leger, S. Rio, E. Monflier, A. Ponchel, *Appl. Catal. A Gen.* **2015**, *506*, 206–219.
- [37] T. Stahlberg, E. Eyjolfssdottir, Y. Y. Gorbanev, I. Sádaba, A. Riisager, *Catal. Letters* **2012**, *142*, 1089–1097.
- [38] F. Wang, L. Jiang, J. Wang, Z. Zhang, *Energy & Fuels* **2016**, *30*, 5885–5892.
- [39] F. C. S. Albonetti, T. Pasini, A. Lolli, M. Blosi, M. Piccinini, N. Dimitratos, J.A. Lopez-Sanchez, D.J. Morgan, A.F. Carley, G.J. Hutchings, *Catal. Today* **2012**, *195*, 120–126.
- [40] A. Villa, M. Schiavoni, S. Campisi, G. M. Veith, L. Prati, *ChemSusChem* **2013**, *6*, 609–612.
- [41] N. K. Gupta, S. Nishimura, A. Takagaki, K. Ebitani, *Green Chem.* **2011**, *13*, 824–827.
- [42] X. Han, L. Geng, Y. Guo, R. Jia, X. Liu, Y. Zhang, Y. Wang, *Green Chem.* **2015**, *18*, 1597–1604.
- [43] S. Siankevich, G. Savoglidis, Z. Fei, G. Laurency, D. T. L.

- Alexander, N. Yan, P. J. Dyson, *J. Catal.* **2014**, *315*, 67–74.
- [44] C. Zhou, W. Deng, X. Wan, Q. Zhang, Y. Yang, Y. Wang, *ChemCatChem* **2015**, *7*, 2853–2863.
- [45] X. Wan, C. Zhou, J. Chen, W. Deng, Q. Zhang, Y. Yang, Y. Wang, *ACS Catal.* **2014**, *4*, 2175–2185.
- [46] G. Yi, S. P. Teong, Y. Zhang, *Green Chem.* **2016**, *18*, 979–983.
- [47] J. Artz, R. Palkovits, *ChemSusChem* **2015**, *8*, 3832–3838.
- [48] Y. Y. Gorbanev, S. Kegnæs, A. Riisager, *Top. Catal.* **2011**, *54*, 1318–1324.
- [49] D. Gu, W. Schmidt, C. M. Pichler, H. J. Bongard, B. Spliethoff, S. Asahina, Z. Cao, O. Terasaki, F. Schüth, *Angew. Chemie - Int. Ed.* **2017**, *8558*, 11374–11377.
- [50] M. Stolarski, J. Walendziewski, M. Steininger, B. Pniak, *Appl. Catal. A Gen.* **1999**, *177*, 139–148.
- [51] B. Liu, R. T. Baker, *J. Mater. Chem.* **2008**, *18*, 5200.
- [52] E. Tani, M. Yoshimura, S. Somiya, *J. Am. Ceram. Soc.* **1983**, *66*, 11–14.
- [53] B.-Q. Xu, J.-M. Wei, Y.-T. Yu, J.-L. Li, Q.-M. Zhu, *Top. Catal.* **2003**, *22*, 77–85.
- [54] W. Ciptonugroho, M. G. Al-Shaal, J. B. Mensah, R. Palkovits, *J. Catal.* **2016**, *340*, 17–29.
- [55] J. Okal, M. Zawadzki, L. Kepiński, L. Krajczyk, W. Tylus, *Appl. Catal. A Gen.* **2007**, *319*, 202–209.
- [56] B. Chen, J. G. Goodwin, Jr., *J. Catal.* **1996**, *158*, 228–235.